Effects of Hydrogen Bonding on the Ring Stretching Modes of Pyridine

Erik R. Berg, Sarah A. Freeman, Daniel D. Green, and Darin J. Ulness*

Department of Chemistry, Concordia College, Moorhead, Minnesota 56562

Received: August 26, 2006; In Final Form: October 8, 2006

The effects of hydrogen bonding on the ring stretching modes (both ring breathing and triangle) of pyridine are experimentally investigated using noisy light based coherent Raman scattering spectroscopy. Three systems, pyridine/formamide, pyridine/water, and pyridine/acetic acid, provide varying degrees of strength for the diluent−pyridine hydrogen bond complex. Formamide forms a relatively weaker hydrogen bond, while acetic acid essentially fully transfers a proton to pyridine. Both dilution studies and temperature studies are performed on the three systems. Together, these provide a broad context in which a very simple model for the electronic behavior of pyridine is formulated. This model is based on a molecular orbital picture and electrostatic arguments, and it well explains the observed experimental results. Additionally, a new mechanism for the line broadening of the ring breathing mode for the pyridine−water hydrogen bonded complex is proposed.

I. Introduction

Hydrogen bonding has been an important and intensely studied subject in chemistry, physics, and biology for what is rapidly approaching a century.[1−3] It is the nature of the hydrogen bond energy that makes it such an interesting and difficult subject to study and understand, as it lies in an intermediate energy range between physical interactions and chemical bonds. The intermediate-strength interaction of the hydrogen bond has been extensively exploited in biological systems. From protein folding to enzymatic activity to neurotransmitter reception, the ability of a system to make and break hydrogen bonds has been key to biological evolution.

The hydrogen bond has been and continues to be studied using any and all methodologies amenable to it. In fact, a very active topic even today is the role of hydrogen bonding in pure water.[4−9] In the area of ultrafast nonlinear optical spectroscopy of liquids, the hydrogen bond, particularly in water but also in other systems, has arguably received the most attention recently. Many research groups using modern ultrafast multidimensional vibrational spectroscopy are directly investigating the impact of hydrogen bonding on the O−H stretching mode in water[8,10−18] and other hydrogen bonding systems.[19−21] These efforts are helping us understand the complicated underlying molecular events that give rise to the broad, nondescript O−H vibrational spectrum typically seen in condensed phase systems.

This work takes a different approach and uses a different method. Here, the ring stretching modes of pyridine (a hydrogen bond acceptor) are studied in the presence of hydrogen bond donors. The method used is noisy light based coherent anti-Stokes Raman scattering (called $I^{(2)}$ CARS). The goal of this work is to study the effects of hydrogen coordination on the ring stretching modes of pyridine. Pyridine has a symmetric ring breathing mode at approximately 990 cm^{-1} and a so-called triangle mode at approximately 1030 cm^{-1}. Both of these modes yield an excellent $I^{(2)}$ CARS signal and are ideally suited for study by this method.

A. Pyridine. Nitrogen heterocycles are ubiquitous in biological systems. Pyridine is one of the simplest nitrogen heterocycles available for study. It has well characterized physical properties and, as mentioned above, has two prominent ring stretching modes that can serve as markers for identifying changes in the electronic environment of pyridine when participating in some biologically important interaction. Pyridine itself is an important component in many powerful pharmaceuticals[22] and biologically important compounds such as nicotine, niacin, vitamin B6, and related compounds. Understanding pyridine and the changes induced upon it during hydrogen bonding should provide insight into many areas of its biochemistry.

Here, we investigate pyridine in the presence of formamide, or water, or acetic acid. The choice of these diluents is to provide a variable degree of hydrogen coordination to the nitrogen. Formamide is a hydrogen bond donor (and also acceptor) through an N−H, whereas water is a donor through an O−H and acetic acid gives up a proton entirely to pyridine to form a pyridinium ion.

It is well-known that the ring breathing mode of pyridine is more strongly perturbed by coordination with hydrogen than the triangle mode.[23−28] It is also the case that the duration of the hydrogen bonded complex is longer than the dephasing time of the vibrational modes. As a result, one observes three distinct peaks in the range 990−1030 cm^{-1} in the presence of a hydrogen bond donor.[23−28] One is the free pyridine ring breathing peak which remains very close to the neat position, another is the ring breathing peak of the hydrogen bonded complex which is shifted to the blue of the neat peak, and the last is the triangle mode where the free and hydrogen bonded peaks are not well resolved. The blue shift of the hydrogen bonded ring breathing mode depends on the nature of the hydrogen bond donor. For (exposed) O−H groups from water or alchohols, the shift is approximately 8 cm^{-1}. For the N−H of formamide, it is about 5 cm^{-1}, and for the case where the

10.1021/jp0655367 CCC: $33.50
Published on Web 11/29/2006

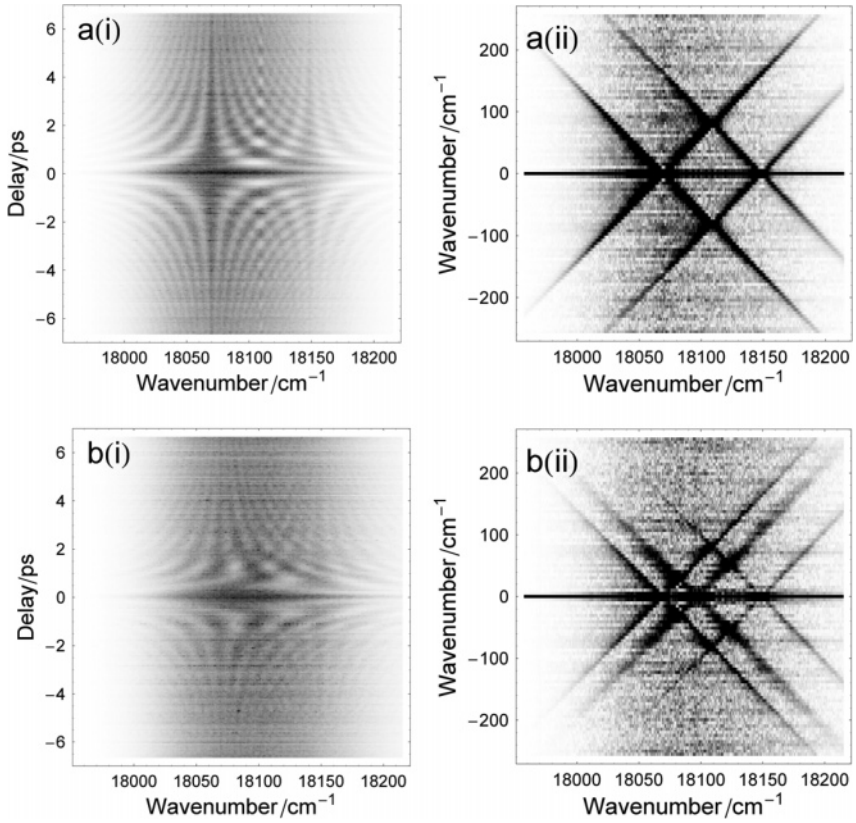

Figure 1. Representative spectrograms (i) and their corresponding Fourier transforms (ii) for (a) neat pyridine and (b) an $X_{py} = 0.6$ mixture of pyridine in acetic acid. In both the spectrograms and the Fourier transformed spectrograms, dark regions represent high I$^{(2)}$CARS signal intensity and light regions represent low signal intensity. The decay of the fringe pattern in the spectrogram is determined by the dephasing rate constants, γ_R, for the Raman active modes. The zero difference frequency, ω_D^0, is the precise detector frequency in which the oscillations in the fringe pattern of the spectrogram, due to a given mode, vanish. On the Fourier transformed spectrograms, the zero difference frequency is the center of the $\times$ pattern. The spectrograms themselves can be fit to eq 2 to yield ultraprecise values for ω_D^0 and highly precise values for γ_R. One can obtain an ultraprecise measurement of the Raman frequency from $\omega_R = (\omega_D^0 - \omega_M)/2$, where ω_M is the frequency of the narrowband laser used to create the I$^{(2)}$CARS signal.

proton is transferred to the pyridine, it is approximately 14 cm^{-1} (see discussion below).

Pyridine is the nitrogen heterocycle analog of benzene. Indeed, the vibrational mode assignment scheme is based on that of benzene.[29,30] Conventionally, the ring breathing mode is labeled ν_1 and the triangle mode is ν_{12}. In benzene, the ring breathing mode has A_{1g} symmetry and the triangle mode has B_{1u} symmetry. The presence of the nitrogen breaks the symmetry from D_{6h} of benzene to C_{2v}. This makes the triangle mode (strongly) Raman active in addition to the ring breathing mode. Both of these modes have A_1 type symmetry in pyridine.

Pyridine principally accepts a hydrogen bond at the nitrogen. Weak hydrogen bond donations can occur with the hydrogens of pyridine, while the π system serves as a point of weak hydrogen bond acceptance.[1] The most stable condition occurs when the hydrogen bond aligns itself with the nitrogen along the C_2 axis; however, in solution at room temperature, a hydrogen bond is considered to be present at angles ranging within a $\pm 30°$ cone around the C_2 axis.[1,31]

B. I$^{(2)}$CARS. I$^{(2)}$CARS is arguably one of the most well developed of the noisy light techniques, and it has exhibited much promise as a probe of ultrafast liquid dynamics.[32−44] Ultrafast time resolution is achieved by exploiting the ultrashort correlation time of noisy laser light in lieu of an ultrashort pulse envelope.[45−47] The "I" in I$^{(2)}$CARS stands for interferometric, an essential aspect of this technique. The superscript "(2)" indicates the use of twin noisy light fields. The technique involves creating twin noisy light fields, B and B′, in an interferometer such that there is a controllable time delay, τ, between the fields. Beams B and B′ have noise profiles that are identical but propagate along distinct wavevectors, $\mathbf{k}_B$ and $\mathbf{k}_{B'}$. These noisy beams are combined, in the standard BOX geometry,[48] with a narrowband field, M (wavevector $\mathbf{k}_M$), and focused into the sample. The frequency of the monochromatic beam is chosen such that it can work in tandem with one of the noisy fields (B or B′) to produce a vibrational coherence. The other noisy field then scatters from the coherence to produce the I$^{(2)}$CARS signal in a four-wave mixing process. This signal is produced with its own wavevector given by the phase-matching condition $\mathbf{k}_{I^{(2)}CARS} = \mathbf{k}_B + \mathbf{k}_{B'} - \mathbf{k}_M$. Because the I$^{(2)}$CARS signal must be frequency dispersed before detection in order to reveal material dynamics, the signal beam is directed into a spectrometer and onto a CCD camera.[39−44]

Detection of the dispersed signal as a function of relative delay, τ, between B and B′ produces a well-known fringe pattern which is observed in the I$^{(2)}$CARS spectrogram.[39−41] By way of example, Figure 1 shows spectrograms for neat pyridine and for a pyridine and acetic acid mixture. These fringes carry a precise relationship to the frequency of the Raman active vibrational transition, ω_R, and usually represent a strong down-conversion of[32−34,42] ω_R. The similarities and differences between noisy light methods and more conventional methods have been thoroughly discussed in the literature.[32−44] The fringes decay with increasing relative interferometric time delay, $|\tau|$,

between noisy beams B and B′. The decay is due to dephasing of the vibrational coherence that has been created at the pump stage by the dual actions of M and one of the broadband fields (B or B′). The dephasing rate constant, γ_R, is determined from the decay of the $I^{(2)}$CARS spectrogram.

The multichannel detection offered by the CCD camera has the very practical advantage of providing a nearly 3 orders of magnitude redundancy in the data. Such very large redundancy provides highly precise measures of these parameters.[39,41,49]

C. Pyridine Mixtures. Of the three mixtures studied in this work, the pyridine/water system has received the most attention in the literature, followed by the pyridine/acetic acid system and finally the pyridine/formamide system. In spite of this, there is not as much literature coverage of the pyridine/water system as perhaps one might expect given the importance and ubiquity of this binary mixture. To be sure, solution thermodynamics of pyridine/water systems was studied long ago[50−53] and continues to appear.[54−57] Evidently, the first computational study was performed by Adam et al. in the late 1960s.[58] There is still active computational work being performed today.[59−64]

In the mid 1980s, a pressure study was performed on aqueous pyridine solutions using Raman spectroscopy.[65] Interestingly, it was the work of Zoidis et al. only a decade ago that was the first careful study of the ring stretching modes of pyridine in water using Raman spectroscopy,[23−24] in spite of the fact that neat pyridine was studied shortly after the discovery of the Raman effect itself.[66] Since then, Schlücker et al. have made important contributions to this area with computational,[25] Raman,[25] and time resolved coherent Raman studies.[26] The work presented here agrees with the findings of these previous studies and compliments that work by (i) employing a different technique ($I^{(2)}$CARS) and (ii) including temperature studies to gain additional insight. Most importantly in this regard, we offer an additional model for line broadening for the ring breathing mode of the hydrogen bonded pyridine−water complex.

In addition to the pyridine/water data, the pyridine/acetic acid and pyridine/formamide experiments provide a wider context for understanding how hydrogen bonding impacts the electronic behavior of pyridine. Computational results are not presented. In lieu of this, a simple intuitive model, based on a molecular orbital picture point of view, and simple electrostatic arguments, is presented. Perhaps surprisingly, this very simple model explains the experimental data well.

Unlike the case of pyridine/water systems, no previous Raman study of pyridine/formamide mixtures could be located by the authors. Some Raman work on the pyridine/acetic acid system has been done, in fact, earlier than that of pyridine/water. Mierzecki[67] in 1964, Singurel and Bazhulin[68] in 1967, and Rezaev and Tabibi[69] in 1976 each present an extensive dilution study for this system. Other non-Raman based work on the pyridine/acetic acid system has been done.[70−72] The pyridine/acetic acid system offers an extra layer of complexity because of the proton transfer that occurs during the acid−base reaction between acetic acid and pyridine.

After this introduction, the experimental procedure is presented. This is followed by an overview of the important results from theoretical work on $I^{(2)}$CARS and a discussion of the data analysis procedure. Results, which include both dilution and temperature studies, are then given for the three systems used. A discussion of the results introduces a very simple model for the electronic behavior of pyridine during hydrogen bonding. Additionally, two principle mechanisms for line broadening of the ring breathing mode of the hydrogen bonded complex are presented. A section summarizing the main results and ideas concludes this work.

II. Experiment

The $I^{(2)}$CARS experiments were performed in the standard way.[39−41] The noisy light source was a modified pumped dye laser (Spectra Physics) containing either kiton red or rhodamine 610 (both from Exciton). In this pumped dye laser, the frequency selective grating was removed and replaced by a simple mirror. This allows the entire lasing spectrum of the dye to be emitted in a phase incoherent way. A second pumped dye laser (Spectra Physics) containing DCM (Exciton), which was operating normally, was used as the narrowband source, M. Both dye lasers were pumped at 10 Hz by a Nd:YAG laser (Spectra Physics).

The noisy beam was split into twin beams, B and B′, by a Michelson interferometer. The length of one arm of the interferometer could be changed via a stepper motor (Newport), which was calibrated using the well characterized $I^{(2)}$CARS signal from benzene. The twin noisy beams emerged from the interferometer running parallel to one another with a separation of approximately 2 mm on-center. The narrowband beam was made to propagate parallel to the noisy beams in the standard BOX beam configuration. The three beams were focused onto the sample using a 150 mm focal length lens. The beam energies at the sample were on the order of tens of microjoules per pulse. The visually apparent $I^{(2)}$CARS signal emerged along its own wavevector and was spatially isolated using an iris. The signal was then directed into a monochromator (SPEX) and ultimately onto a 100 × 1340 pixel array, liquid-nitrogen-cooled CCD detector (Roper Scientific/Princeton Instruments). This spectral dimension of the experiment was calibrated using neon lines. The absolute resolution of the spectrometer, as characterized by the half-width at half-maximum of the neon lines, was found to be 0.38 cm^{-1}. $I^{(2)}$CARS spectra were collected at each delay setting to produce the spectrogram. All spectrograms were produced by moving the stepper motor over a range from −1.00 to 1.00 mm in steps of 0.01 mm. At each delay, a ten-shot average spectrum was recorded. Four complete spectrograms were averaged for each sample. Each spectrogram took approximately 8 min to acquire.

The samples were pyridine, glacial acetic acid, formamide (all from Acros), and distilled water (obtained locally). All samples were used as received with no further purification. Mole fraction mixtures, of approximately 15 mL total volume, were created using either class A burets or graduated pipets. The error in mole fraction is estimated to be less than 0.7%. Temperature control of the samples was done using a home-built brass jacket and a recirculating bath (FTS Systems). The temperature was held constant to within ±0.2 °C. During the experiment, the samples were contained in a 2 mm glass cuvette (Starna) with a Teflon stopper. Despite the stopper, a small amount of evaporation of the sample was noted at high temperature settings. The operating assumption was that this evaporation did not significantly change the mole fractions of the components in the solution over the duration of the data aquisition runs.

III. Theory and Data Analysis

The theory of $I^{(2)}$CARS has been treated extensively elsewhere.[33,41,42] Here, we present only the important results from previous theoretical treatments of $I^{(2)}$CARS.

A. Results from I$^{(2)}$CARS Theory. The analytic results for the I$^{(2)}$CARS signal, $I(\omega_D, \tau)$, as a function of detected frequency, ω_D, and interferometric delay time, τ, are presented here. The material response function is taken to decay exponentially (Lorentzian line shape), and the noisy light is taken to have a Lorentzian spectral density. For the situation in which there is a mixture of one type of molecule, a, which exhibits a single vibrational resonance in the vicinity of $\omega_R = \omega_B - \omega_M$, and another type of molecule, b, which has no overlapping resonance, the frequency- and delay-time-dependent I$^{(2)}$CARS signal intensity is given by

$$\begin{aligned} I(\omega_D, \tau) \propto {} & X_a^2\langle\gamma_a^R\rangle^2\gamma^2 J(\Delta_1)\, J(-\Delta_2) \exp\{-2\gamma|\tau|\} \times \\ & \left(\frac{\cos(\Delta_{CARS}\tau)}{2\gamma} + \frac{\sin(\Delta_{CARS}|\tau|)}{\Delta_{CARS}}\right) + \\ & 2J(\Delta_1)\, J(-\Delta_2)[X_a^2\langle\gamma_a^R\rangle\langle\gamma_a^N\rangle\gamma + X_aX_b\langle\gamma_a^R\rangle\langle\gamma_b^N\rangle\gamma] \times \\ & \exp\{-2\gamma|\tau|\} \sin(\Delta_{CARS}|\tau|) + 2K(\omega_D)[X_a^2\langle\gamma_a^N\rangle^2 + \\ & 2X_aX_b\langle\gamma_a^N\rangle\langle\gamma_b^N\rangle + \mathbf{X}_b^2\langle\gamma_b^N\rangle^2] \times \exp\{-2\Gamma|\tau|\} \\ & \left(\cos(\Delta_R\tau) + \frac{2\Gamma}{\Delta_R}\sin(\Delta_R|\tau|)\right) + I(\omega_D, \infty) \quad (1) \end{aligned}$$

where $I(\omega_D, \infty)$ is the τ-independent background term. In this expression, $J(\Delta_i)$ is the spectral density of the broadband light, where $\Delta_1 = \bar{\omega}_B - \omega_M - \omega_R$ is the radiation−resonance detuning frequency constant in the step that prepares the vibrational coherence, and $\Delta_2 = \bar{\omega}_B - \omega_D + \omega_R$ is the resonance−detection detuning frequency in the step that probes this coherence for detected frequency, ω_D. The variable $\bar{\omega}_B$ is the carrier frequency of the noisy light. $K(\omega_D)$ is the spectral density of the purely nonresonant component of the signal. X_a and X_b are the mole fractions of a and b, and $\langle\gamma_a^R\rangle$, $\langle\gamma_a^N\rangle$, and $\langle\gamma_b^N\rangle$ are, respectively, the common elements of the third-order orientationally averaged hyperpolarizability tensor for the resonant and nonresonant contributions of a and the nonresonant contribution of[36] b. $\Delta_{CARS} = 2\omega_R + \omega_M - \omega_D$, where ω_M is the frequency of the monochromatic beam. The frequency Δ_{CARS} vanishes at the zero difference frequency, ω_D^0; here, $\omega_R = (\omega_D^0 - \omega_M)/2$ precisely gives the Raman vibrational frequency. The observed decay rate constant is $\gamma = \gamma_R + (\gamma_I/2)$, where the instrument response, γ_I, is due to a finite slit width of the monochromator and a finite bandwidth of the monochromatic beam. Γ is the (Lorentzian) bandwidth of the broadband fields.

Three classes of terms appear in (1): (i) fully resonant (a−a only), (ii) two types of resonant−nonresonant (a−a and a−b), and (iii) three types of fully nonresonant (a−a, a−b, and b−b). For the case of pyridine, where there is more than one active mode, the extension of expression 1 is straightforward, since, in I$^{(2)}$CARS, each mode acts independently.

B. Data Fitting. With the multipeak version of expression 1 as the guide from theory, the I$^{(2)}$CARS spectrograms for each of the pyridine mixtures were fit to the equation

$$I(\omega_D,\tau) = AJ'(\omega_D)\begin{cases} e^{-2\gamma_1|\tau-\tau_0|}(\cos[(\omega_{D_1}^0 - \omega_D)|\tau-\tau_0|] + R_1 \sin[(\omega_{D_1}^0 - \omega_D)|\tau-\tau_0|]) \\ + A_2 e^{-2\gamma_2|\tau-\tau_0|}(\cos[(\omega_{D_2}^0 - \omega_D)|\tau-\tau_0|] + R_2 \sin[(\omega_{D_2}^0 - \omega_D)|\tau-\tau_0|]) \\ \vdots \\ + A_i e^{-2\gamma_3|\tau-\tau_0|}(\cos[(\omega_{D_i}^0 - \omega_D)|\tau-\tau_0|] + R_i \sin[(\omega_{D_i}^0 - \omega_D)|\tau-\tau_0|]) \\ + I_0 + m(\tau-\tau_0) \end{cases} \quad (2)$$

using Mathematica which employs the Marquardt−Levenberg version of nonlinear least-squares regression.[73,74] τ_0 is a fit parameter representing the absolute zero delay time, which corresponds to perfect temporal overlap of the noise patterns in B and B′ where they overlap spatially in the sample. In eq 2, A is a fit parameter representing the overall amplitude of the signal and A_i is the ratio of the amplitude of mode i to mode 1. The fit parameters $R_i = 4\langle\gamma_{eff}^N\rangle/\langle\gamma_i^R\rangle$, where $\langle\gamma_{eff}^N\rangle$ is the effective nonresonant hyperpolarizability of the solutution, measure the ratio of the amplitudes of the terms that are odd in Δ_{CARS} (the nonresonant−resonant cross term) to the term that is even in Δ_{CARS} (the purely resonant term). The fit parameters $\omega_{D_i}^0$ are the zero difference frequencies for mode i. Since for I$^{(2)}$CARS $\omega_{D_i}^0 = \omega_M + 2\omega_{R_i}$, the Raman frequency is determined by $\omega_{D_i}^0$ provided ω_M is accurately known and the signal detection window is correctly calibrated. For frequency shifts, ω_M need not be calibrated, so any uncertainty associated with ω_M does not appear in the shift measurements, an advantage of the method. The fit parameters γ_i measure the empirical decay rate constant of the interferometric fringes. Theory dictates that the spectrum $J'(\omega_D)$ be the spectrum of the broadband beam blue shifted by one vibrational frequency. We take $J'(\omega_D)$ to be the empirically measured spectrum of the signal derived from a sample containing only the resonant species ($X_{py} = 1$). Empirical eq 2 represents a simplification of (1) in which the purely nonresonant term is neglected. This is justified because we include only data for which $|\tau| \gg 1/\Gamma$ in the fitting procedure. Although the fit parameters are not strictly orthogonal, they are highly insensitive to one another;[49] therefore, the reliability of one of the extracted parameters is only very mildly impacted by the reliability of the other parameters. Of the three physically relevant parameters extracted from the fit—ω_R, γ_R, and R—by far, the most precisely recovered is[41,49] ω_R followed by γ_R and finally R. The relative error in ω_R can be as low as 2×10^{-3}% for the I$^{(2)}$CARS method.[41,49] The relative error on γ_R and R can be as low as 5 and 10%, respectively.[41,49]

It is important to note that the I$^{(2)}$CARS spectrograms yield a precise measure of the parameters of eq 2. The accuracy of eq 2 itself and the absolute accuracy of the I$^{(2)}$CARS measurement is no better than any more conventional technique.

C. X-Marginal Spectra. As mentioned above, data are collected in the form of a spectrogram. In addition to the massive data redundancy responsible for the extreme precision of the I$^{(2)}$CARS process, the spectrogram method of detection provides a valuable visual representation of the signal. This is particularly true of the Fourier transformed version of the spectrogram (Figure 1b). The visually apparent × pattern in the transformed spectrogram allows one to unambiguously see Raman modes that are not evident in the raw spectrogram nor would be strongly present in a spectrum representation. As valuable as this is, the Fourier transformed spectrograms suffer from the fact that it is difficult to compare one transformed spectrogram to another in anything other than a very gross qualitative way.

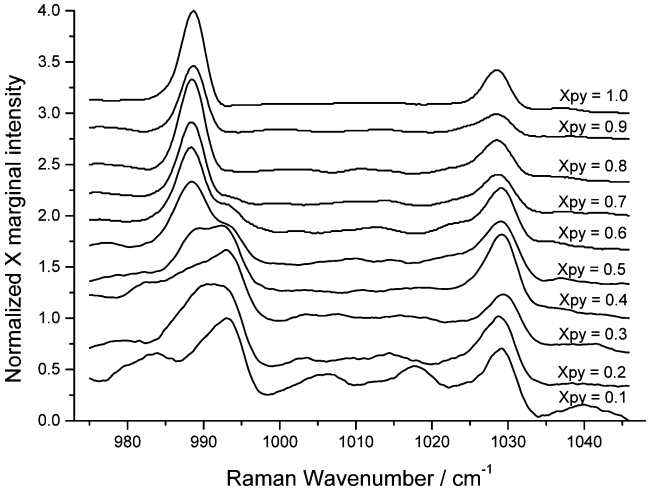

Figure 2. x-Marginal spectra for the 10 different mole fraction solutions used in the dilution study of the pyridine/formamide system. The spectra are normalized to range between zero and unity. A constant offset has been added to stack the spectra for visual clarity. The quality of the x-marginal spectra decreases with lower Raman resonant contribution to the $I^{(2)}$CARS signal which occurs as X_{py} decreases.

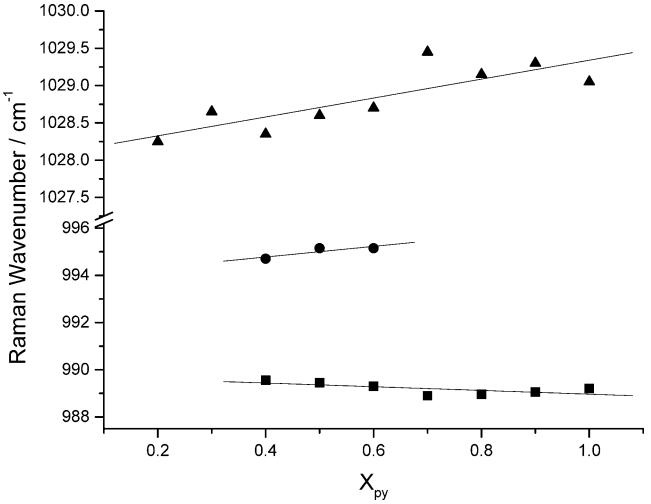

Figure 3. Fit results for the Raman wavenumber values for the ring breathing mode of free pyridine (squares), the ring breathing mode of the hydrogen bonded complex (circles), and the triangle mode (triangle), for the pyridine/formamide system. The parameters (slope, intercept) for the best fit lines are the following: free pyridine ring breathing mode (−0.786, 989.75), hydrogen bonded complex ring breathing mode (2.250, 993.87), and triangle mode (1.267, 1028.07).

It is therefore valuable to compress the visual information carried by the two-dimensional picture of the Fourier transformed spectrogram into a one-dimensional spectrum. This is done by computing what is called the x-marginal.[44] The motivation of the x-marginal procedure is to imitate what the human eye does in recognizing the characteristic × pattern of a Raman mode. A narrow (0.6 cm^{-1}) ×-shaped mask is defined such the that slopes of the lines making up the × mask match the slopes of the × pattern of the Raman mode (slopes equal 1 and −1 when both axes of the transformed spectrogram are in wavenumber units). The mask has a value of unity within the defined × shape and zero outside of it. The Fourier transformed spectrogram is multiplied by the mask leaving nonzero values within the × area. The result is then summed up to give a single value called the x-marginal. The center of the mask is then moved to the adjacent pixel value, and the procedure is repeated to give another x-marginal value. When the × mask is centered over an ×-shaped Raman mode, the x-marginal is large; conversely, when the × mask is not centered over the Raman mode, the x-marginal is small (but not zero) As the center position of the × is scanned across the Fourier transformed spectrogram, a collection of x-marginals is collected to form an x-marginal spectrum.

It is important to keep in mind the x-marginal spectra do not provide precise quantitative data regarding the parameters of the material model. Quantitative data are obtained from fitting the spectrograms themselves. The x-marginal spectra simply provide a concise qualitative representation of the data contained in the spectrograms. The x-marginal representation of the data is more thoroughly discussed in the Supporting Information associated with this work.

IV. Results

A. Dilutions with Formamide. The x-marginal spectra for the 10 different mole fraction solutions of formamide and pyridine used in the dilution study are shown in Figure 2. Two distinct peaks persist from the neat pyridine state to a mole fraction of $X_{py} = 0.6$ where a clear shoulder develops approximately 5 cm^{-1} to the blue of the free pyridine ring breathing peak. This corresponds to the ring breathing mode for the hydrogen bonded complex. At a mole fraction of $X_{py} = 0.4$, the magnitude of the ring breathing peak of the hydrogen bonded complex exceeds that of the free pyridine. The triangle mode appears, in the x-marginal spectra, to remain relatively unchanged during the dilution process.

The fit results from applying eq 2 for the Raman vibrational frequency are shown in Figure 3. The wavenumber value of the free ring breathing mode blue shifts very slightly (0.47 cm^{-1}) upon dilution with formamide from neat to $X_{py} = 0.4$. There is perhaps a nonlinearity to the trend, but this cannot be concluded with a high degree of confidence. There is a slight (0.45 cm^{-1}) red shifting of the ring breathing mode of the hydrogen bonded complex in going from a mole fraction of $X_{py} = 0.6$ to $X_{py} = 0.4$. Unfortunately, due to the convoluted nature of this peak with the free ring breathing peak, low Raman resonant signal contribution at small X_{py}, and the small amount of hydrogen bonded complex at high X_{py}, only three values of ω_R for this mode could be obtained with ultrahigh precision. The triangle mode experiences a red shift of 1.00 cm^{-1} upon dilution from neat to $X_{py} = 0.2$. Again, because of the convolution of the free ring breathing peak and the ring breathing peak from the hydrogen bonded complex, high precision extractions of γ_R and R could not be obtained for this data series.

Figure 4 collects the x-marginal spectra for a temperature study of an $X_{py} = 0.4$ mixture of formamide and pyridine. The temperature ranges from −40 to 60 °C with data taken every 20 °C. A clear change in the ring breathing peaks at 989 cm^{-1} and 994 cm^{-1} is seen. The peaks become more resolved and spread apart as the temperature is lowered from 60 to −40 °C. Additionally, the free pyridine state is favored at high temperatures and the hydrogen bonded state is favored at low temperatures, indicative of the exothermic nature of the hydrogen bonding between formamide and pyridine. The triangle mode appears relatively unchanged through the temperature range. Ultraprecise fits of these data (Figure 5) show that the free pyridine ring breathing mode blue shifts by 0.77 cm^{-1}/100 °C, while the hydrogen bonded complex ring breathing mode red shifts by 0.89 cm^{-1}/100 °C. The triangle mode does indeed remain essentially constant with perhaps a very slight (0.36 cm^{-1}) red shift being suggested by the data.

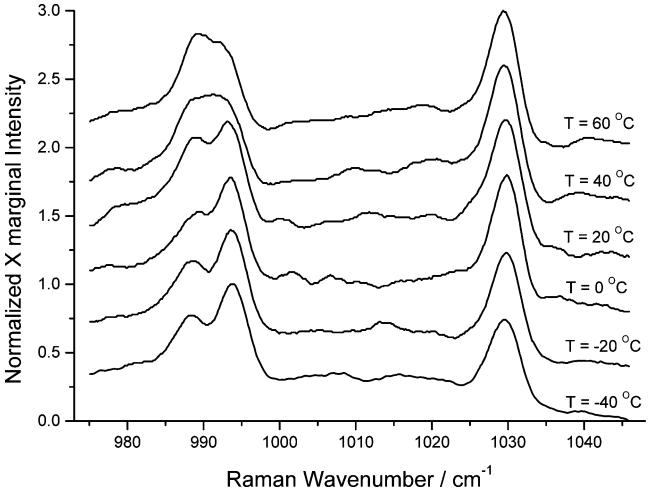

Figure 4. x-Marginal spectra for an $X_{py} = 0.4$ mixture of pyridine and formamide. The spectra are normalized to range between zero and unity. A constant offset is added to stack the spectra for visual clarity.

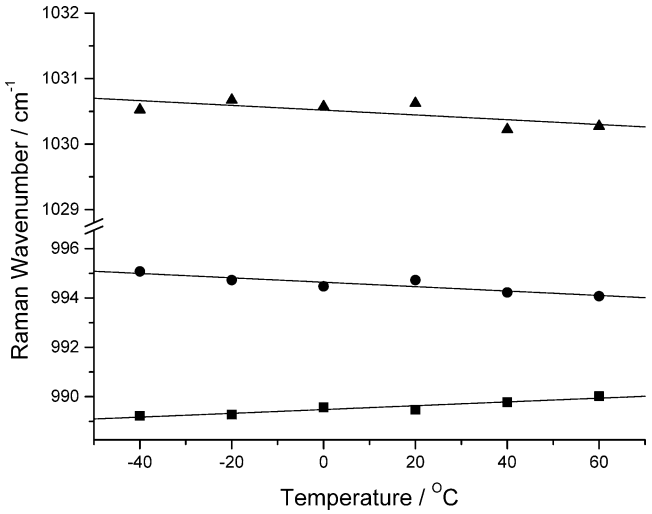

Figure 5. Wavenumber values for the free pyridine ring breathing mode (squares), hydrogen bonded complex ring breathing mode (circles), and triangle mode (triangles) obtained by fitting to eq 2. The parameters (slope, intercept) for the best fit lines are the following: free pyridine ring breathing mode (0.008, 989.48), hydrogen bonded complex ring breathing mode (−0.009, 994.64), and triangle mode (−0.004, 1030.52).

B. Dilutions with Water. As with formamide, 10 different mole fraction mixtures of water and pyridine were studied and their x-marginals are shown in Figure 6. In this set of spectra, the ring breathing mode for the hydrogen bonded complex appears at around 997 cm^{-1} which is 8 cm^{-1} to the blue of the ring breathing mode of the free pyridine. There is a relatively rapid transition from the case where free pyridine is the dominant form of the pyridine to when the hydrogen bonded complex is in excess. Figure 6 shows a dramatic difference between $X_{py} = 0.6$ and $X_{py} = 0.5$. The triangle mode appears relatively unchanged during the dilution process, although a slight shoulder may be appearing on the low energy side of the peak.

Fitting to eq 2 provides ultraprecise tracking of changes in the Raman frequency for the three modes present in the x-marginals. Because the peaks are better separated, reliable fits could be obtained for lower $I^{(2)}$CARS signal values. Fit results are collected in Figure 7a. The free pyridine ring breathing mode exhibits a slight red shift of 0.42 cm^{-1} upon dilution with water from the neat state to $X_{py} = 0.5$; the shift

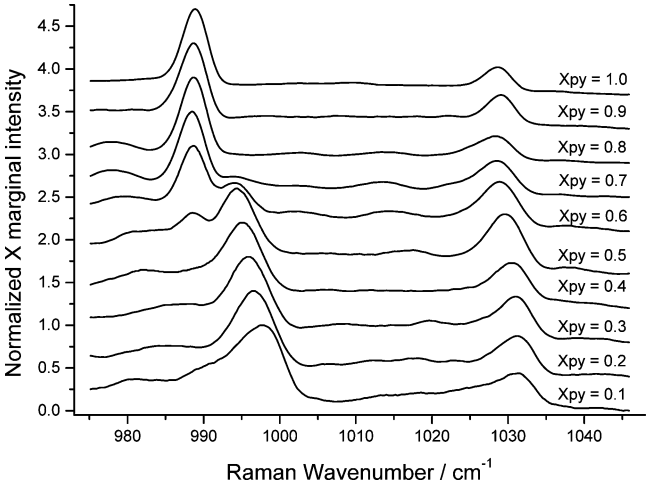

Figure 6. x-Marginal spectra for the 10 mole fraction solutions used in the dilution study of the pyridine/water system. The spectra are normalized to range between zero and unity. A constant offset has been added to stack the spectra for visual clarity. The quality of the x-marginal spectra decreases with lower Raman resonant contribution to the $I^{(2)}$CARS signal which occurs as X_{py} decreases.

appears to be linear. The ring breathing vibration for the hydrogen bonded complex experiences a more complicated shift in frequency. There is ultimately a blue shifting as the complex becomes more and more dominant (low X_{py}); however, the shift is not linear and there appears to be a slight red shift that initially occurs. Interestingly, the lowest energy vibration appears to be at the mole fraction where the free and hydrogen bonded pyridines are in equal amounts ($X_{py} \sim 0.55$). The triangle mode also experiences a blue shift that is not linear with the greatest rate of change occurring at low X_{py}. It is likely that this shift is somewhat artificial because of the emergence of a separate peak.[23−28] The fitting of the convoluted modes to a single-exponential decay would not be appropriate.

Figure 7b shows values for γ_R for the ring breathing modes of the free and hydrogen bonded complex. The free pyridine mode experiences a decrease of the dephasing rate constant upon dilution, whereas the hydrogen bonded complex experiences an increase in the dephasing rate constant. As mentioned above, the triangle mode may well be a convolution of distinct modes. Data for γ_R for this mode (not shown) are consistent with this idea in that they are more scattered than those for the other modes and there is an abrupt increase from the neat state.

These pyridine/water results are consistent with previous studies. Zoidis et al.[23,24] report a blue shift of ∼7 cm^{-1} for the ring breathing mode upon hydrogen bonding. They treat the ring breathing mode of the hydrogen bonded complex as a pair of modes (see discussion below) and assign distinct peak widths to each (∼2.3 and ∼1.8 cm^{-1}). In the current work, the mode is treated as a single vibration, so expectedly, a larger width is reported (Figure 7b). Schlücker et al.[25−26] report a blue shift of ∼6 cm^{-1} for the ring breathing mode of the hydrogen bond complex relative to the free pyridine case. They also report a line width of ∼3 cm^{-1} that is a decreasing function of X_{py}.

The temperature study results in the form of x-marginals are shown in Figure 8. Here, an $X_{py} = 0.55$ mole fraction solution of pyridine and water is studied over a temperature range of −40 to 60 °C with data taken every 20 °C. As with formamide, the hydrogen bonding process is exothermic and entropically unfavorable as high temperatures favor the free state and low temperatures favor the hydrogen bonded state. The triangle mode appears relatively unchanged. More careful analysis using results from fitting to eq 2 show (see Figure 9a) that, as with

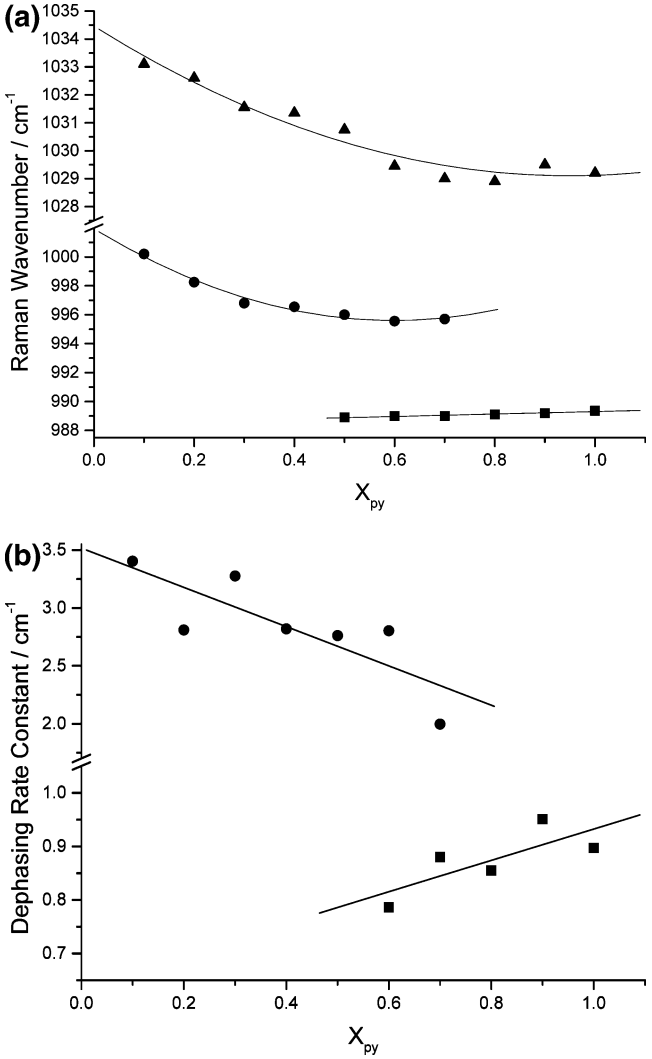

Figure 7. (a) Fit results for the Raman wavenumber values for the ring breathing mode of free pyridine (squares), the ring breathing mode of the hydrogen bonded complex (circles), and the triangle mode (triangles) for the pyridine/water system. The line of best fit parameters (slope, intercept) for free pyridine ring breathing mode is (0.843, 988.46). The second-order polynomial best fit parameters (quadratic, linear, constant) are the following: hydrogen bonded complex ring breathing mode (17.738, −21.226, 1001.95) and triangle mode (5.947, −11.293, 1034.47). (b) Fit results for the dephasing rate constant for the ring breathing mode of free pyridine (squares) and the ring breathing mode of the hydrogen bonded complex (circles), for the pyridine/water system. The lines of best fit parameters (slope, intercept) are the following: free pyridine ring breathing mode (0.293, 0.639) and hydrogen bonded complex ring breathing mode (−1.696, 3.517).

formamide, the ring breathing frequencies for the free and hydrogen bonded states separate as the temperature is lowered. Unlike with formamide, however, the free ring breathing mode remains essentially constant over the temperature range and only the ring breathing frequency of the hydrogen bonded complex blue shifts by 1.18 cm^{-1}/100 °C as the temperature is lowered. The triangle mode changes with temperature (−0.85 cm^{-1}/100 °C) as well, but perhaps not in a linear fashion.

The dephasing rate constants for the free ring breathing and triangle modes of pyridine in water are shown in Figure 9b. The free ring breathing rate constant increases by 0.4 cm^{-1}/100 °C, while the triangle mode rate constant decreases (−0.62 cm^{-1}/100 °C). The dephasing rate constant for the hydrogen bonded complex for pyridine in water increases by 0.33 cm^{-1}/100 °C.

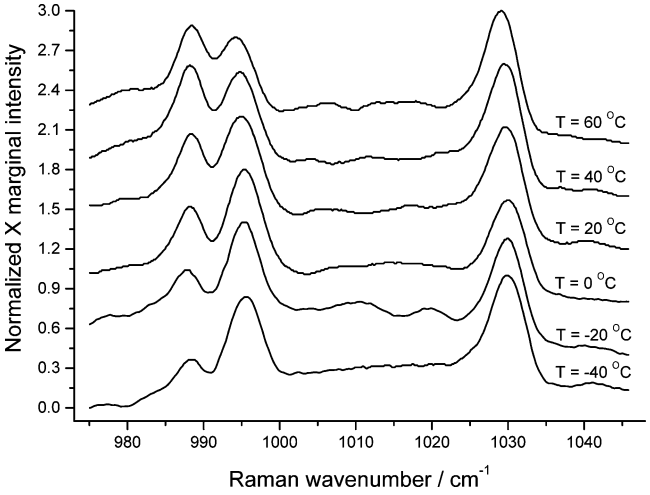

Figure 8. x-Marginal spectra for an $X_{py} = 0.55$ mixture of pyridine and water. The spectra are normalized to range between zero and unity. A constant offset is added to stack the spectra for visual clarity.

C. Dilutions with Acetic Acid. Figure 10 shows the x-marginal spectra for 13 of the 20 different mole fraction mixtures of pyridine and acetic acid studied here. As expected, at high X_{py} values the "free" pyridine ring breathing and triangle peaks are dominant. As X_{py} is lowered, a new ring breathing peak attributed to the pyridinium cation ring breathing peak appears approximately 14 cm^{-1} blue shifted from the free pyridine peak. No new triangle peak is observed, but the relative amplitude of this peak decreases. At intermediate values of X_{py}, the pyridinium cation ring breathing peak is the dominant feature, with the relative amplitude of pyridine peaks decreasing further. A new triangle peak begins to emerge at $X_{py} = 0.5$.

An interesting result occurs at very low values of X_{py}. A new ring breathing peak appears approximately 15 cm^{-1} blue shifted from the main pyridinium cation peak. The appearance of this peak suggests that the dominant peak at 1004 cm^{-1} is that of a relatively long-lived ionic pair complex (pyridinium cation/acetate anion). It can be inferred that the new peak at 1019 cm^{-1} is the ring breathing peak of the free pyridinium cation. This interpretation is consistent with the idea that at intermediate mole fractions there is a large amount of both pyridinium cations and, therefore, acetate anions present in solution. Thus, there is a high likelihood that nearly every pyridinium cation has an acetate anion as one of its nearest neighbors. However, as X_{py} falls to small values, there is an overwhelming number of intact acetic acid molecules present. Therefore, in spite of the fact that the ionic pair is presumably significantly more stable, a non-negligible fraction of pyridinium cations have no acetate anion as a nearest neighbor. Why this should result in a blue shift from the pyridinium cations having an acetate anion partner with which to complex will be discussed below. The ion pair complex is evidently longer lived than 6 ps (and perhaps much longer) as the observed peaks are distinct.

These findings are consistent with both the work of Mierzacki[67] and Singurel and Bazhulin.[68] Both these works report a dominant new peak that is blue shifted ∼15−17 cm^{-1} from the ring breathing peak of free pyridine. Both works also report a weak peak developing at low X_{py} values. Meirzacki attributes this to water contamination.[67] Singurel and Bazhulin suggest, as the current authors do, that the dominant peak is from a pyridine cation−acetate anion pair complex and the weak peak is from the free pyridinium ion.[68]

Another interesting feature of the acetic acid dilution is the strong suppression of the triangle mode. This is much more

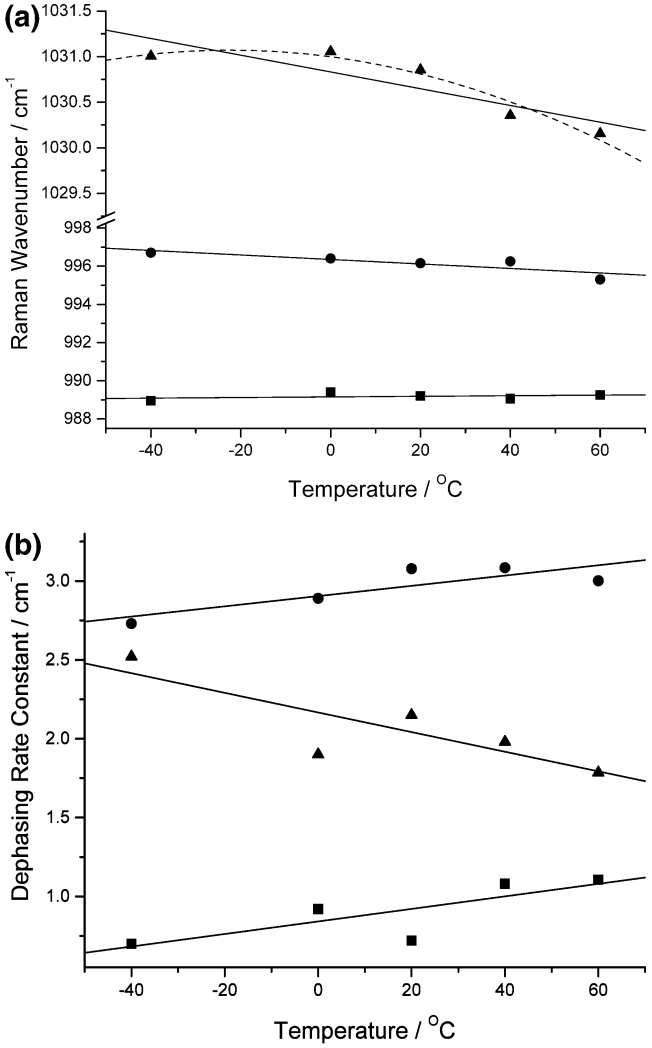

Figure 9. (a) Fit results for the Raman wavenumber values for the ring breathing mode of free pyridine (squares), the ring breathing mode of the hydrogen bonded complex (circles), and the triangle mode (triangles), for the pyridine/water system. The parameters (slope, intercept) for the best fit lines are the following: free pyridine ring breathing mode (0.002, 989.15), hydrogen bonded complex ring breathing mode (−0.0118, 996.35), and triangle mode (0.009, 1030.80). The data for the triangle mode were also fit to a second-order polynomial. The best fit parameters (quadratic, linear, constant) for the triangle mode are (−0.000146, −0.00652, 1031.00). (b) Fit results for the dephasing rate constant for the ring breathing mode of free pyridine (squares), the ring breathing mode of the hydrogen bonded complex (circles), and the triangle mode (triangles) for the pyridine/water system. The parameters (slope, intercept) for the best fit lines are the following: free pyridine ring breathing mode (0.00398, 0.842), hydrogen bonded complex ring breathing mode (−0.00623, 2.167), and triangle mode (0.00325, 2.905).

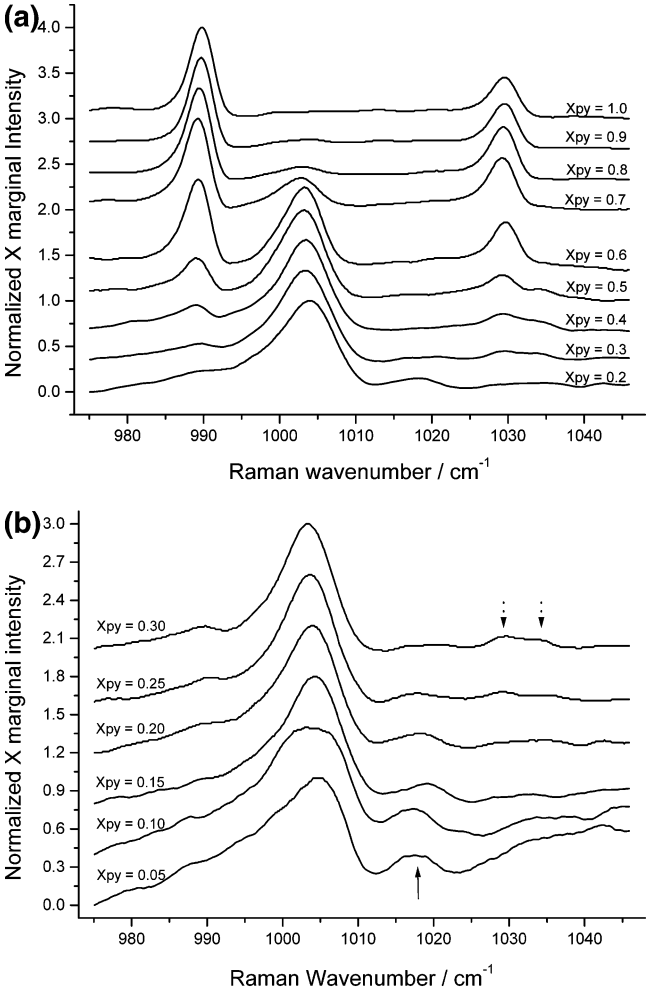

Figure 10. x-Marginal spectra for 13 of the different mole fraction solutions used in the dilution study of the pyridine/acetic acid system. Part a shows high to moderately low X_{py} values, and part b shows the low X_{py} regime. The spectra are normalized to range between zero and unity. A constant offset has been added to stack the spectra for visual clarity. The quality of the x-marginal spectra decreases with lower Raman resonant contribution to the $I^{(2)}$CARS signal which occurs as X_{py} decreases. The dashed arrows identify the disappearing triangle peaks, and the solid arrow points to the emerging free pyridinium ion peak.

dramatic than the case of the mixture with water or formamide. A rigorous explanation of this behavior cannot be given here; however, a heuristic argument can be made. The pyridinium cation is very similar in structure to benzene. Benzene has D_{6h} symmetry, so its triangle mode (B_{1u}) is not Raman active by symmetry. The pyridinium cation is still a member of the C_{2v} point group, so one cannot rigorously use symmetry to explain the strong suppression of the triangle mode. Nonetheless, the "benzene-like" nature of the pyridinium cation might underlie the observed results.

The raw four-run averaged $I^{(2)}$CARS spectrograms for the pyridine/acetic acid dilution series were fit using eq 2. The results are shown in Figure 11. Figure 11a shows the Raman wavenumbers for the ring breathing modes of pyridine and the ion paired pyridinium cation as a function of the mole fraction of pyridine. The changes are very subtle, as a free pyridine peak has what might be a red shift of less than 0.07 cm^{-1}. A red shift is more resolvable for the pyridinium cation and it is not linear with the maximum red shift of 2.8 cm^{-1} occurring at $X_{py} = 0.55$ and returning to nearly the original value at small mole fractions of pyridine. Figure 11b shows the Raman wavenumber of the triangle mode. Here, as with the free pyridine, there is no discernible trend. Unfortunately, the fits become less reliable for this mode at higher mole fractions than for the ring breathing mode. The dephasing rate constant (in units of wavenumbers) is shown in Figure 11c. There, values for the free pyridine ring breathing mode and triangle modes are very well behaved. Interestingly, they both exhibit a slight positive curvature in their trendlines and both exhibit mild increases in size as X_{py} decreases. The fit values for the pyridinium ion pair complex are more varied but nonetheless show a significant increase in value as the mole fraction of pyridine is decreased.

The raw four-run averaged $I^{(2)}$CARS spectrograms for the pyridine/acetic acid temperature study were also fit using eq 2.

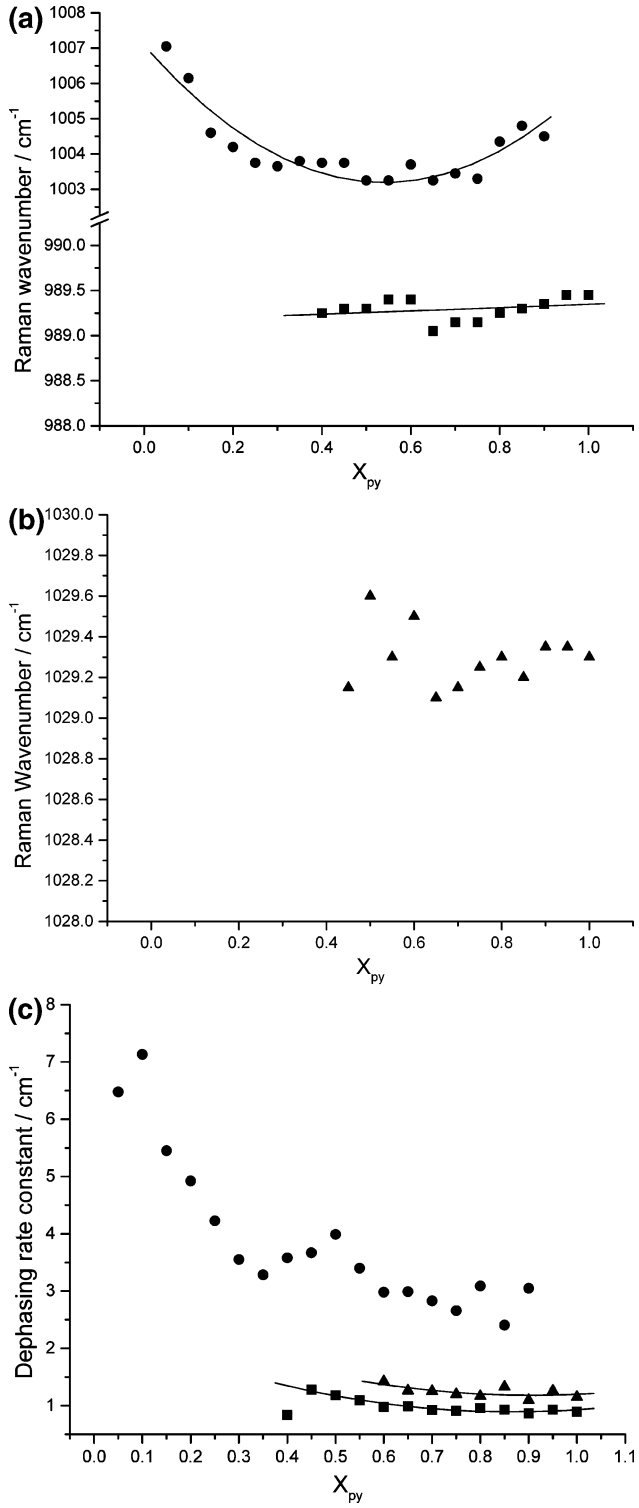

Figure 11. Fit results for (a) the Raman wavenumber values for the ring breathing mode of free pyridine (squares), the ring breathing mode of the pyridinium cation (circles), and (b) the triangle (triangles) mode for the pyridine/acetic acid system. The line of best fit parameters (slope, intercept) for free pyridine is (0.181, 989.17). The second-order polynomial of best fit parameters (quadratic, linear, constant) for the pyridinium cation is (13.293, −14.378, 1007.08). The line of best fit parameters (slope, intercept) for the triangle mode is (−0.073, 1029.3). (c) Fit results for the dephasing rate constant values for the ring breathing mode of free pyridine (squares), the pyridinium cation (circles), and the triangle mode (triangles) for the pyridine/acetic acid system. The second-order polynomials of best fit parameters (quadratic, linear, constant) are the following: free pyridine ring breathing mode (2.095, −3.630, 2.462), the pyridinium cation ring breathing mode (8.475, −12.242, 7.204), and the triangle mode (2.006, −3.633, 2.826).

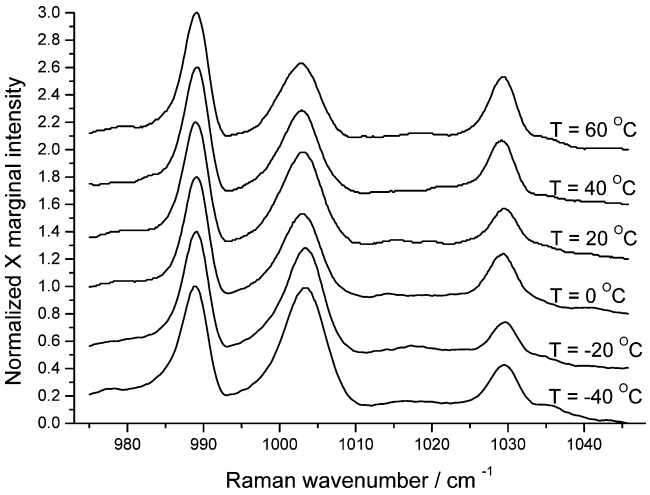

Figure 12. x-Marginal spectra for an $X_{py} = 0.6$ mixture of pyridine and acetic acid. The spectra are normalized to range between zero and unity. A constant offset is added to stack the spectra for visual clarity.

The x-marginal spectra are shown in Figure 12. An $X_{py} = 0.60$ solution was used, and data at several temperatures between −40 and 60 °C were taken. Figure 12 shows the Raman wavenumbers for the ring breathing modes of both pyridine and the pyridinium ion pair complex and the triangle mode of pyridine. The frequency of the ring breathing mode of pyridine is essentially independent of temperature, whereas the pyridinium ion pair complex and the triangle mode of pyridine each exhibit a slight red shift with increasing temperature, approximately 1.06 cm^{-1}/100 °C for the former and 0.27 cm^{-1}/100 °C for the latter (Figure 13a and b). Interestingly, as shown in Figure 13c, it is the pyridinium ion pair complex that has a temperature-independent dephasing rate constant, while both the ring breathing and triangle modes have dephasing rate constants that decrease with increasing temperature. No discernible trend was seen in the nonresonant to resonant hyperpolarizability ratio (data not shown).

D. Thermodynamic Information. The thermodynamic values $\Delta G^{\ominus}$, $\Delta H^{\ominus}$, and $\Delta S^{\ominus}$ can be obtained for the systems studied here. The most convenient reference state to employ is Rauolt's law reference where the equilibrium constant is defined as

$$K_X = \frac{X_{\text{py-D}}}{X_{\text{py}} X_{\text{D}}}$$

where D stands for the hydrogen bond donar. $I^{(2)}$CARS is not optimally suited for extracting very precise thermodynamic values. Nevertheless, it is valuable to present the thermodynamic information contained in these data, realizing that other methods might provide more precise measures of these values in the future. The Supporting Information associated with this work discusses how thermodynamic information is extracted from $I^{(2)}$CARS data. Figure 14 shows $\Delta G^{\ominus}$ as a function of temperature for the three systems studied here, and Table 1 summarizes the results.

The values for $\Delta G^{\ominus}$, $\Delta H^{\ominus}$, and $\Delta S^{\ominus}$ are significantly smaller in magnitude than those reported for cases where the hydrogen bonding pair are solutes in a non-hydrogen bonding solvent. This is intuitive. That $\Delta S^{\ominus} < 0$ is because of the association occurring in the hydrogen bonding process. This would be larger in magnitude in the presence of a non-hydrogen bonding solvent. Without the non-hydrogen bonding solvent, nonassociated water (or formamide) molecules are nevertheless likely to be hydrogen bonded to other water (formamide) molecules. One also expects

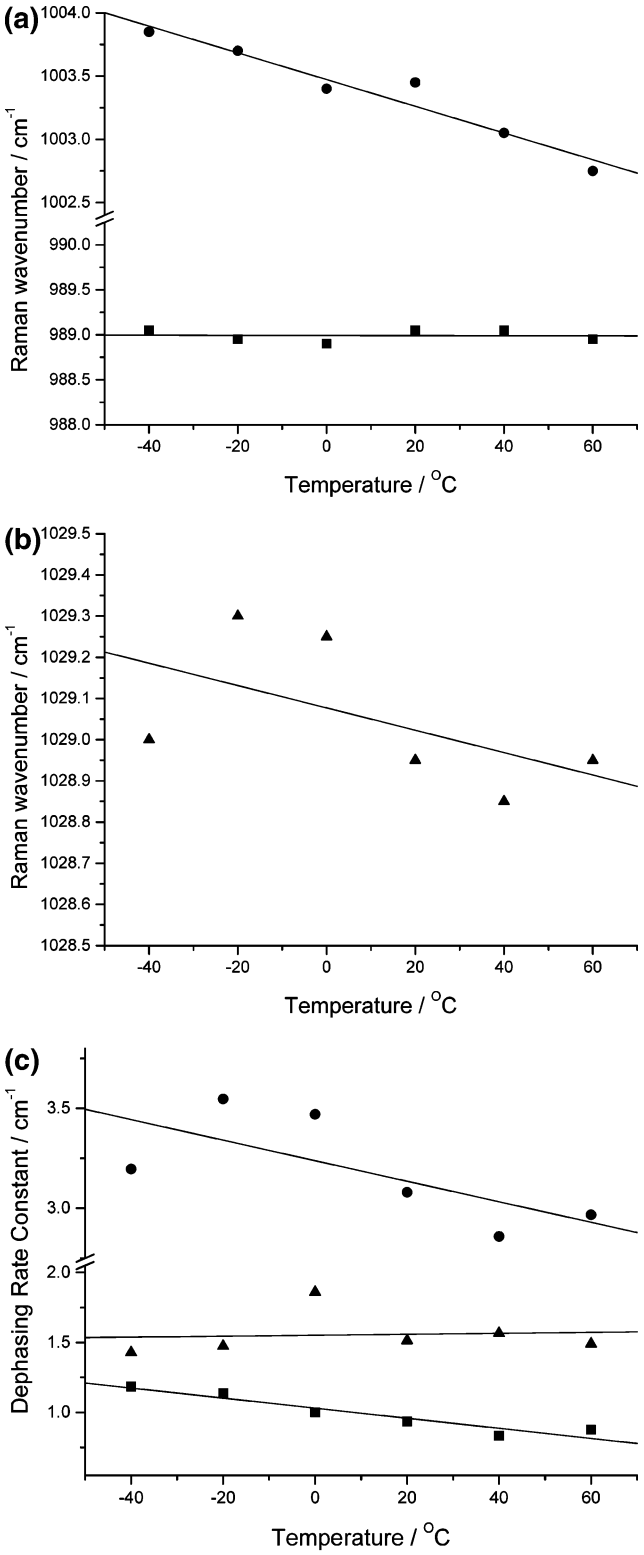

Figure 13. Wavenumber values for the (a) free pyridine ring breathing (squares), the ring breathing mode of the pyridinium cation (circles), and (b) the triangle mode (triangles) obtained by fitting to eq 2. The parameters (slope, intercept) for the best fit lines are the following: free pyridine (0.000714, 988.992), pyridinium cation (−0.0106, 1003.472), and triangle mode (−0.0027, 1024.077). (c) Fit results for the dephasing rate constant values for the ring breathing mode of free pyridine (squares), the ring breathing mode of pyridinium cation (circles), and the triangle mode (triangles) for the pyridine/acetic acid system. The parameters (slope, intercept) for the best fit lines are the following: the free pyridine ring breathing mode (−0.004, 1.030), the pyridinium cation ring breathing mode (−0.005, 3.238), and the triangle mode (0.003, 1.552).

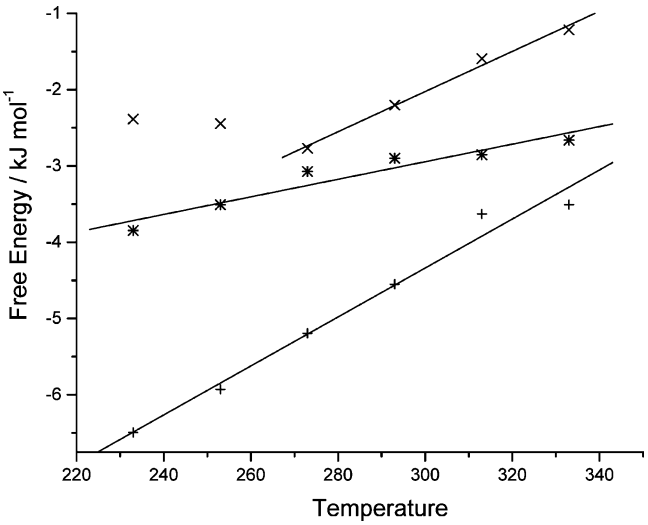

Figure 14. $\Delta G^{\ominus}$ as a function of temperature for the three systems included in this work. Pyridine/water (+) shows a relatively linear trend ($R^2 = 0.98$ for fit) resulting in $\Delta H^{\ominus} = -13.97$ kJ/mol and $\Delta S^{\ominus} = -32$ J/(mol·K). Pyridine/acetic acid (∗) also shows a linear trend ($R^2 = 0.92$ for fit), yielding $\Delta H^{\ominus} = -6.40$ kJ/mol and $\Delta S^{\ominus} = -12$ J/(mol·K). The two lowest temperature data points for the pyridine/formamide (×) system do not follow the linear behavior of the higher temperature data (see text). Only the data from $T = 273-333$ K were included in the fit ($R^2 = 0.99$). This gives $\Delta H^{\ominus} = -9.92$ kJ/mol and $\Delta S^{\ominus} = -26$ J/(mol·K). Care must be taken when comparing these values to others reported in the literature (see text for discussion).

TABLE 1: Thermodynamic Values for Hydrogen Bonding/ Proton Transfer for the Three Systems Included in This Work as Determined from the Data Shown in Figure 14[a]

quantity	pyridine/ formamide	pyridine/ water	pyridine/ acetic acid
$\Delta G^{\ominus}$ (298 K)	−2.08 kJ/mol	−4.41 kJ/mol	−2.97 kJ/mol
$\Delta H^{\ominus}$	−9.92 kJ/mol	−13.97 kJ/mol	−6.40 kJ/mol
$\Delta S^{\ominus}$	−26 J/(mol·K)	−32 J/(mol·K)	−12 J/(mol·K)

[a] The Raoult law reference state is used. The values must be interpreted as describing both the dissociation of the donor−donor interaction and the association of the donor−pyridine interaction.

the $\Delta H^{\ominus}$ value to be smaller in magnitude because, without the non-hydrogen bonding solvent, formation of the pyridine−donor complex requires breakage of donor−donor hydrogen bonds. Thus, the thermodynamic values presented here should not be interpreted as referring solely to the hydrogen bonding process between pyridine and the donor but must also include the breaking of donor−donor complexes. To summarize the results, the entire hydrogen bonding process for pyridine/water systems and pyridine/formamide systems is energetically favorable and entropically unfavorable. The two lowest temperature data points for the pyridine/formamide system fall completely out of line with the remainder of the data. It is not presently clear whether the data are erroneous due to the difficulty posed by the convolution of the mode peaks or if it is indicative of some physical process occurring at low temperatures. These two data points were not included in the linear fit. The thermodynamic data for the pyridine/acetic acid system must be viewed as

$$H_3CCOOH + Py \rightleftharpoons H_3CCOO^- \cdots HPy^+$$

where the three-dot symbol represents the ion pair complex between the pyridinium cation and the acetate anion.

E. Neat Pyridine. The $I^{(2)}$CARS data collected here provide a measure of the absolute Raman frequencies of the ring stretching modes for neat pyridine in addition to measurement

of the dephasing rate constant and the resonant to nonresonant hyperpolarizability ratio. Although ultraprecise measurements of frequency shifts can be obtained, absolute measurements also include a calibration of the narrowband source which lessens the precision somewhat. For the ring breathing mode, $\omega_R = 989.35 \pm 0.16\ cm^{-1}$, $\gamma_R = 0.86 \pm 0.05\ cm^{-1}$, and $\langle\gamma_{eff}^N\rangle/\langle\gamma_i^R\rangle = 0.094 \pm 0.009$, and for the triangle mode, $\omega_R = 1029.18 \pm 0.13\ cm^{-1}$, $\gamma_R = 1.16 \pm 0.06\ cm^{-1}$, and $\langle\gamma_i^R\rangle/\langle\gamma_{eff}^N\rangle = 0.137 \pm 0.02$.

V. Discussion

The pyridine mixtures with formamide, water, and acetic acid represent varying degrees of "hydrogen bondedness". With N−H as a donor in formamide, the hydrogen bond with the nitrogen of pyridine is relatively weak. The strength of the hydrogen bond increases with the O−H donor of water. Finally, with acetic acid, the hydrogen forms an actual bond with pyridine to form the pyridinium cation.

The results presented in this work and those of the literature show that the pyridine ring breathing mode is blue shifted by hydrogen coordination and the stronger the hydrogen bond, the greater the blue shift. The triangle mode is much less perturbed by hydrogen bonding. A blue shifting of the ring breathing mode suggests a tightening of the bonds within pyridine. That the triangle mode is not significantly blue shifted suggests that the tightening of the bonds are due to a strengthening of the delocalized π character of bonds as opposed to the localized sigma character of the individual bonds.

A. Simple Model of Electronic Behavior in Pyridine. A simple model of the electronic behavior of pyridine upon hydrogen bonding can be made using a qualitative molecular orbital picture. The model presented below is clearly a gross oversimplification of changes in electron distribution in pyridine; nonetheless, it provides a simple picture that seems to be consistent with all of the results of this work.

Without the hydrogen bond, free pyridine has a lone pair of electrons in an sp^2 hybrid orbital localized on the nitrogen atom. Due to the relatively large spatial extent of the orbitals of the nonbonded lone pair electrons, the delocalized π molecular orbital gets "squeezed" out of the region and this destabilizes the π contribution to the ring bonds relative to a hypothetical situation where there is no lone pair of electrons on the nitrogen. When hydrogen bonding occurs, some of the lone pair electron density gets drawn out by the hydrogen, thereby releasing the "squeeze" on the π orbital. This allows better delocalization of the π electron density and stabilizes the system resulting in a blue shift of the ring breathing mode. Figure 15 expresses the essential aspects of the model in pictorial form.

The fact that the blue shift increases from formamide to water to acetic acid is consistent with this qualitative picture. A stronger hydrogen bond will draw out more of the lone pair electron density. This relieves the squeezing of the π molecular orbital to a greater degree, causing more stabilization and a greater blue shift. This picture is also consistent with the assignment of the dominant ring breathing peak of the pyridinium cation to an ion pair complex and that of the smaller and "bluer" peak to free pyridinium cation ring breathing. The presence of the acetate anion near the hydrogen attached to the nitrogen in the pyridinium cation draws back the partial positively charged hydrogen to some degree. This weakens the coordination to the nitrogen relative to that when no anion is present. On the basis of the current qualitative argument, the ion pair complex should then have a ring breathing mode that is to the red of the free pyridinium cation.

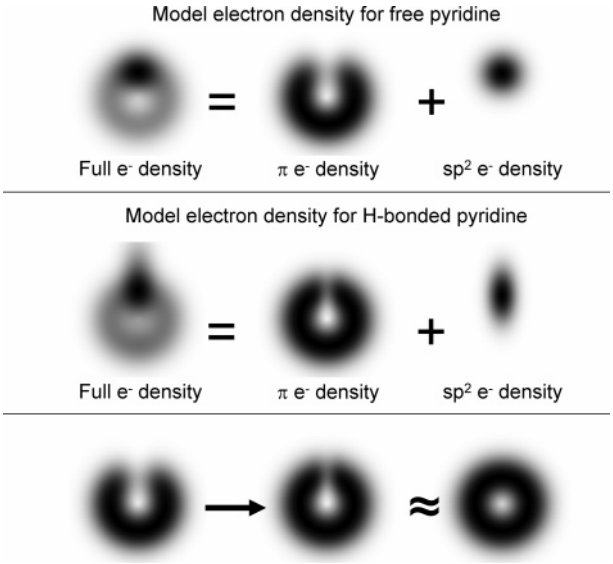

Figure 15. Simple molecular orbital based description of the electronic behavior of pyridine upon hydrogen bonding. The density plots are purely illustrative; there is no connection to any numerical calculation. The electron density for benzene is represented by a torus. Pyridine has a lone pair of electrons occupying an sp^2 orbital. This squeezes out electron density of the π system (exaggerated in picture for visual clarity). When hydrogen bonding occurs, some of the sp^2 electron density is drawn out by the incoming hydrogen. This releases π electron density somewhat, making it more like the fully delocalized π electrons of benzene. This simple model seems to well explain the experimental data presented in this work (see text). This includes the central result that the ring breathing mode is significantly blue shifted upon hydrogen bonding, whereas the triangle mode is not affected to nearly the same degree.

B. Line Broadening Mechanisms. All of the diluents used in this work are rather complicated liquids because each is both a hydrogen bond donor and acceptor. This allows for complicated networks of transient clusters held together by hydrogen bonds to exist throughout the liquid. In the important and careful work on Raman spectra from pyridine and water systems by Zoidis et al.[23,24] and also by Schlücker et al.,[25,26] these networks were considered as primary causes for the line broadening of the ring breathing mode of the hydrogen bonded complex relative to that of free pyridine. Several different hydrogen bond complex stoichiometries where deemed as most important: PyW, Py_2W, PyW_2, and PyW_3. Those authors were careful to acknowledge, however, that, for a binary mixture, without an inert (non-hydrogen bonding) cosolvent, assignment of distinct stoichiometries is likely not to be appropriate and a continuum of bands is more likely the case.[23]

It is proposed here that, for the case of water as the diluent, the network mechanism and the various stoichiometries are not the primary source of line broadening but they are likely a secondary source. The primary mechanism proposed here is based on the thermalized distribution of the direct hydrogen bond between water and pyridine. The potential energy well is very broad and shallow for the hydrogen bond between water and pyridine,[1,31] so even though the most stable energy configuration is at a fixed hydrogen bond distance and angle, a wide range of lengths and angles are well within the thermal energy of the optimum configuration.[1,31] Thus, there is a high Boltzmann probability that a generic pyridine−water pair will not be in the optimum configuration. This spread in the configuration of the pyridine−water pairs across the ensemble is proposed as the chief broadening mechanism.

The grounds for this proposed mechanism is in the work of Fileti et al.[31] in which a Monte Carlo based computational study of pyridine in water was performed. Although the computation was for the case of very dilute pyridine, the basic results are broadly applicable. They report simulation results in which 17% of pyridine showed no hydrogen bonding, 62% showed a single hydrogen bond, 20% two hydrogen bonds, and 1% three hydrogen bonds. In addition to purely energetics, they concluded that the proton acceptor site (the nitrogen) experiences a great deal of local thermal disorder and, in the liquid state, many configurations are governed by temperature and natural disorder.[31] (Figure 3 of Fileti et al. is particularly illustrative.[31])

It is the temperature study that provides a point of differentiation between the thermalized distribution hypothesis and the network hypothesis. The network hypothesis suggests a decrease in line width of the ring breathing mode for the hydrogen bonded complex as temperature is increased because increasing the temperature disrupts the network clusters, reducing the efficiency in channeling away the vibrational coherence. The thermal distribution hypothesis, on the other hand, suggests an increase in line width as the temperature is increased because a broader range of water−pyridine pair configurations would be accessible. The temperature data in Figure 9b show an increasing line width. Other data for the water/pyridine system are consistent with the thermalized distribution picture. Figure 9a shows a blue shift of the ring breathing frequency for the hydrogen bonded complex as the temperature is reduced. In light of the simple molecular orbital based picture discussed above, this is to be expected. At lower temperature, only the more stable hydrogen bond configurations contribute. These are the stronger of the bonds, so this should emphasize the blue side of the distribution of ring breathing frequencies. There is also evidence in support of the network mechanism as playing a role in broadening in addition to the thermalized distribution mechanism. Figure 7b shows an increase in line width of the ring breathing mode for the hydrogen bonded complex with increasing diluent concentration. At high water levels, more potential network clusters can be formed and this could explain the increase in line width as X_{py} goes down.

The broadening mechanism for the acetic acid/pyridine system is more difficult to understand, but it is speculated here that in this case the network mechanism is primary for the ion pair complex ring breathing peak. This suggestion is supported by the temperature data in Figure 13c which show an increase in line width at lower temperatures. It is also supported by the data in Figure 11c which show an increasing line width with increasing diluent concentration.

VI. Conclusions

This work provides experimental results for the $I^{(2)}$CARS signal from the ring stretching modes of pyridine in pyridine/formamide, pyridine/water, and pyridine/acetic acid binary mixtures. Both dilution and temperature studies were performed. The ultraprecise measurement of vibrational frequency shifts and dephasing rate constants, a virtue of the $I^{(2)}$CARS technique, provides further insight into the underlying physical mechanisms that impact the ring stretching modes of pyridine upon hydrogen bonding.

A very simple model employing molecular orbital pictures and electrostatic arguments was able to explain the experimental results while providing an intuitive picture of the impact on hydrogen bonding on pyridine. Dephasing rate constant measurements provide experimental grounds for the line broadening of the ring breathing mode for the hydrogen bonded complex in water. This model was based on the idea of a thermalized distribution of hydrogen bond configurations. This model complements the existing understanding in the literature which emphasizes the transient network of water. The temperature study allowed for thermodynamic values to be extracted for the pyridine/water and pyridine/formamide systems.

Acknowledgment. We thank Lindsay R. Weisel, Thao M. Ta, and Eric C. Booth for preliminary data on pyridine and water systems. Brittany G. Berger and Zachary C. Johnson provided valuable assistance with data analysis. We also thank Donald Krogstad, Drew Rutherford, and Mark Gealy for valuable discussion. We are grateful to Tony Pietrzak and computer services at Concordia College for use of the computer laboratory for data analysis. This work was supported by NSF CAREER grant CHE-0341087, the Dreyfus Foundation, and the Concordia College Chemistry Research Endowment.

Supporting Information Available: Discussion on x-marginal spectra and thermodynamic information. This material is available free of charge via the Internet at http://pubs.acs.org.

References and Notes

(1) Jeffrey, G. A. *An Introduction to Hydrogen Bonding*; Oxford University Press: New York, 1997.

(2) Vinogradov S. N.; Linnell, R. H. *Hydrogen Bonding*; Van Nostrand Reinhold: New York, 1971.

(3) Pimentel, G. C.; McClellan, A. L. *The Hydrogen Bond*; W.H. Reeman: San Fransisco, CA, 1960.

(4) Wernet, Ph.; Nordlund, D.; Bergmann, U.; Cavalleri, M.; Odelius, M.; Ogasawara, H.; Näslund, L. Å.; Hirsch, T. K.; Ojamäe, L.; Glatzel, P.; Pettersson, L. G. M.; Nilsson, A. *Science* **2004**, *304*, 995.

(5) Smith, J. D.; Cappa, C. D.; Wilson, K. R.; Messer, B. M.; Cohen, R. C.; Saykelly, R. J. *Science* **2004**, *306*, 851.

(6) Head-Gordon, T.; Johnson, M. E. *Proc. Natl. Acad. Sci. USA* **2006**, *103*, 7973.

(7) Zubavicus, Y.; Grunze, M. *Science* **2004**, *304*, 974−976.

(8) Asbury, J. B.; Steinel, T.; Stromberg, C.; Corcelli, S. A.; Lawrence, C. P.; Skinner, J. L.; Fayer, M. D. *J. Phys. Chem. A* **2004**, *108*, 1107.

(9) Smith, J. D.; Cappa, C. D.; Wilson, K. R.; Messer, B. M.; Cohen, R. C.; Geissler, P. L.; Saykelly, R. J. *Proc. Natl. Acad. Sci. USA* **2005**, *102*, 14171.

(10) Yeremenko, S.; Pshenichnikov, M. S.; Wiersma, D. A. *Phys. Rev. A* **2006**, *73*, 021804.

(11) Eaves, J. D.; Loparo, J. L.; Fecko, C. J.; Roberts, S. T.; Tokmakoff, A; Geissler, P. L. *Proc. Natl. Acad. Sci. USA* **2005**, *102*, 13019.

(12) Fecko, C. J.; Loparo, J. L.; Roberts, S. T.; Tokmakoff, A. *J. Chem. Phys.* **2005**, *122*, 054506.

(13) Gelin, M. F.; Kosov, D. S. *J. Chem. Phys.* **2006**, *124*, 144514.

(14) Harder, E.; Eaves, J. D.; Tokmakoff, A.; Berne, B. J. *Proc. Natl. Acad. Sci. USA* **2005**, *102*, 11611.

(15) Steinel, T.; Asbury, J. B.; Corcelli, S. A.; Lawrence, C. P.; Skinner, J. L.; Fayer, M. D. *Chem. Phys. Lett.* **2004**, *386*, 295.

(16) Wang, Z.; Pakoulev, A.; Pang, Y.; Dlott, D. D. *J. Phys. Chem. A* **2004**, *108*, 9054.

(17) Wang, Z.; Pakoulev, A.; Pang, Y.; Dlott, D. D. *Chem. Phys. Lett.* **2003**, *378*, 281.

(18) Laenen, R.; Rauscher, C.; Lubereau, A. *J. Phys. Chem. B* **1998**, *102*, 9304.

(19) Ha, J.-H.; Kim, Y. S.; Hochstrasser, R. M. *J. Chem. Phys.* **2006**, *124*, 064508.

(20) Gómez Marigliano, A. C.; Varetti, E. L. *J. Phys. Chem. A* **2002**, *106*, 1100.

(21) Fecko, C. J.; Eaves, J. D.; Tokmakoff, A. *J. Chem. Phys.* **2002**, *117*, 1139.

(22) Bell, T. W.; Khasanov, A. B.; Drew, M. G. B. *J. Am. Chem. Soc.* **2002**, *124*, 14092.

(23) Zoidis, E.; Yarwood, J.; Danten, Y.; Besnard, M. *Mol. Phys.* **1995**, *85*, 373.

(24) Zoidis, E.; Yarwood, J.; Danten, Y.; Besnard, M. *Mol. Phys.* **1995**, *85*, 385.

(25) Schlücker, S.; Singh, R. K.; Asthana, B. P.; Popp, J.; Kiefer, W. *J. Phys. Chem A* **2001**, *105*, 9983.

(26) Schlücker, S.; Heid, M.; Singh, R. K.; Asthana, B. P.; Popp, J.; Kiefer, W. Z. *Phys. Chem.* **2002**, *216*, 267.

(27) Kreyenschmidt, M.; Eysel, H. H.; Asthana, B. P. *J. Raman Spectrosc.* **1993**, *24*, 645.
(28) Asthana, B. P.; Takahashi, H.; Kiefer, W. *Chem. Phys. Lett.* **1983**, *94*, 41.
(29) Kline, C. H., Jr.; Turkevich, J. *J. Chem. Phys.* **1944**, *12*, 300.
(30) Corrsin, L.; Fax, B. J.; Lord, R. C. *J. Chem. Phys.* **1953**, *21*, 1170.
(31) Fileti, E. E.; Countinho, K.; Malaspina, T.; Canuto, S. *Phys. Rev. E* **2003**, *67*, 061504.
(32) Dugan, M. A.; Mellinger, J. S.; Albrecht, A. C. *Chem. Phys. Lett.* **1988**, *147*, 411.
(33) Dugan, M. A.; Albrecht, A. C. *Phys. Rev. A* **1991**, *43*, 3877.
(34) Dugan, M. A.; Albrecht, A. C. *Phys. Rev. A* **1991**, *43*, 3922.
(35) Schaertel, S. A.; Albrecht, A. C.; Lau, A.; Kummrow, A. *Appl. Phys. B* **1994**, *59*, 377.
(36) Schaertel, S. A.; Lee, D.; Albrecht, A. C. *J. Raman Spectrosc.* **1995**, *59*, 889.
(37) Kozich, V. P.; Lau, A.; Pfeiffer, M.; Kummrow, A. *J. Raman Spectrosc.* **1999**, *30*, 473.
(38) Lau, A.; Kummrow, A.; Pfeiffer, M.; Woggon, S. *J. Raman Spectrosc.* **1994**, *25*, 607.
(39) Stimson, M. J.; Ulness, D. J.; Albrecht, A. C. *Chem. Phys. Lett.* **1996**, *263*, 185.
(40) Ulness, D. J.; Kirkwood, J. C.; Stimson, M. J.; Albrecht, A. C. *J. Chem. Phys.* **1997**, *107*, 7127.
(41) Ulness, D. J.; Stimson, M. J.; Albrecht, A. C. *Chem. Phys.* **1997**, *222*, 17.
(42) Ulness, D. J. *J. Phys. Chem. A* **2003**, *107*, 8111.
(43) Aung, P. P.; Cosert, K. M.; Weisel, L. R.; Schulz, T. F.; Gealy M. W.; Ulness D. J. *J. Raman Spectrosc.* **2005**, *36*, 409.
(44) Weisel, L. R.; Ta, T., Booth, E. C.; Ulness, D. J. *J. Raman Spectrosc.*, in press.
(45) Morita, N.; Yajima, T. *Phys. Rev. A* **1984**, *30*, 2525.
(46) Nakatsuka, N.; Tomita, M.; Fujiwara, M.; Asaka, S. *Phys. Rev. A* **1984**, *29*, 2286.
(47) Beach, R.; Hartmann, S. R. *Phys. Rev. Lett.* **1984**, *53*, 663.
(48) Shirley, J. A.; Hall, R. J.; Eckbreth, A. C. *Opt. Lett.* **1980**, *5*, 380.
(49) Dawlaty, J. M.; Ulness, D. J. *J. Raman Spectrosc.* **2001**, *32*, 211.
(50) Pucher, G.; Dehn, W. M. *J. Am. Chem. Soc.* **1921**, *43*, 1753.
(51) Jones, W. J.; Speakman, J. B. *J. Am. Chem. Soc.* **1921**, *43*, 1867.
(52) Andon, R. J.; Cox, J. D. *J. Chem. Soc.* **1952**, 4601.
(53) Andon, R. J.; Cox, J. D.; Herington, E. F. G. *J. Chem. Soc.* **1954**, 3188.
(54) Abe, J.-I.; Nakanishi, K.; Touhara, H. *J. Chem. Thermodyn.* **1978**, *10*, 483.
(55) Matteoli, E.; Lepori, L. *J. Chem. Phys.* **1984**, *80*, 2856.
(56) Brovchenko, I. V.; Oleinkova, A. V. *J. Chem. Phys.* **1997**, *106*, 7756.
(57) Johnson, J. R.; Kilpatrick, P. J.; Christian, S. D.; Affsprung, H. E. *J. Phys. Chem.* **1968**, *72*, 3223.
(58) Adam, W.; Grimison, A.; Hoffmann, R.; de Ortiz, C. Z. *J. Am. Chem. Soc.* **1968**, *90*, 1509.
(59) Berezin, K. V.; Nechaev, V. V. Zotov, S. N. *J. Struct. Chem.* **2004**, *45*, 388.
(60) Sicilia, M. C.; Niño, A.; Muñoz-Caro, C. *J. Phys. Chem. A* **2005**, *109*, 8341.
(61) Malaspina, T.; Countinho, K.; Canuto, S. *J. Chem. Phys*. **2002**, *117*, 1692.
(62) Cai, Z.-L.; Reimers, J. R. *J. Phys. Chem. A* **2002**, *106*, 8769.
(63) Dkhissi, A.; Adamowicz, L.; Maes, G. *J. Phys. Chem. A* **2000**, *104*, 2112.
(64) Pápai, I.; Janscó, G. *J. Phys. Chem. A* **2000**, *104*, 2132.
(65) Zakin, M. R.; Grubb, S. G.; King, H. E., Jr.; Herschbach, D. R. *J. Chem. Phys.* **1986**, *84*, 1080.
(66) Venkateswaran, S. *J. Phys. Chem.* **1930**, *34*, 145.
(67) Mierzecki, R. *Acta Phys. Pol.* **1960**, *19*, 41 (in French).
(68) Singurel, L.; Bazhulin, P. A. *Vestn. Mosk. Gos. Univ. Ser. Fiz. Aston.* **1967**, *1*, 11 (in Russian).
(69) Rezaev, N. I.; Tabibi, M. B. *Russ. Phys. J.* **1976**, *19*, 1159.
(70) Pei, K.; Li, Y.; Li, H. *J. Mol. Struct.* **2003**, *660*, 113.
(71) Ventatesan, V. K.; Suryanarayana, C. V. *J. Phys. Chem.* **1956**, *60*, 777.
(72) Chawla, B.; Mehta, S. K. *J. Phys. Chem.* **1984**, *88*, 2650.
(73) Press, W. H.; Flannery, B. P.; Teukolsky, S. A.; Vetterling, W. T. *Numerical Recipes in C: The Art of Scientific Computing*, 2nd ed.; Cambridge University Press: New York, 1992.
(74) Wolfram, S. *Mathematica 3.0 Standard Add-on Packages*; Cambridge University Press: New York, 1996.